Single-root networks for describing the potential energy surface of Lennard-Jones clusters

Yinjiang Cai (蔡引江), and Longjiu Cheng (程龙玖)

Citation: The Journal of Chemical Physics **149**, 084102 (2018); doi: 10.1063/1.5043330
View online: https://doi.org/10.1063/1.5043330
View Table of Contents: http://aip.scitation.org/toc/jcp/149/8
Published by the American Institute of Physics

Single-root networks for describing the potential energy surface of Lennard-Jones clusters

Yinjiang Cai (蔡引江) and Longjiu Cheng (程龙玖)[a)]
School of Chemistry and Chemical Engineering, Anhui University, Hefei, Anhui 230601, People's Republic of China

(Received 8 June 2018; accepted 9 August 2018; published online 24 August 2018)

Potential energy surface (PES) holds the key in understanding a number of atomic clusters or molecular phenomena. However, due to the high dimension and incredible complexity of PES, only indirect methods can be used to characterize a PES of a given system in general. In this paper, a branched dynamic lattice searching method was developed to travel the PES, which was described in detail by a single-root network (SRN). The advantage of SRN is that it reflects the topological relation between different conformations and highlights the size of each structure energy trap. On the basis of SRN, to demonstrate how to transform one conformation to another, the transition path that connects two local minima in the PES was constructed. Herein, we take Lennard-Jones (LJ) clusters at the sizes of 38, 55, and 75 as examples. It is found that the PES of these three clusters have many local funnels and each local funnel represents one morphology. If a morphology is located more frequently, it will lie in a larger local funnel. Besides, certain steps of the transition path were generated successfully, such as changing from icosahedral to truncated octahedral of the LJ_{38}-cluster. Though we do not exhibit all the parts of the PES or all transition paths, this method indeed works well in the local area and can be used more widely. *Published by AIP Publishing.* https://doi.org/10.1063/1.5043330

I. INTRODUCTION

Potential energy surface (PES) is a major issue in many fields such as molecular dynamics,[1–6] protein folding,[7–15] and transition state theory.[16–19] The understanding of a reaction is also based on the knowledge of the PES by finding its reaction path.[20] Actually, PES is a multidimensional surface which represents the relationship between energy of the system and the positions of all atoms.[21] The number of PES features like local minima, transition states, and pathways increases exponentially when the size of the cluster increases.[22–26] The main problem is the hardness to characterize PES directly because of the high dimension of PES. To better understand the PES intuitively, many methods gave the abstract shape of PES like the three-dimensional graph or complex network.[27–33] Considering the degree of complexity, these methods simplify the PES by keeping a certain aspect of it, and different methods focus on different aspects. The most widely used method is disconnectivity graph[30] which connects the all local minima in the PES.[29,34] By mapping the full conformation space into the set of local minima, disconnectivity graph partitions conformation space into energy-dependent or temperature-dependent basins and achieves good results. The corrugation-reducing method based on the observation that most of the corrugation in a molecule-surface PES is already embedded in the atom-surface interactions constructs a six-dimensional PES.[28] The one-dimensional free-energy profile method uses an additive function of the nodes on either side of the minimum cut. The resulting profile gives the free energy as a function of the progress coordinate.[27] In these methods, the high-dimension PES was projected onto lower dimensions, which might be highly misleading.[35]

Another important issue in theoretical chemistry is the finding of transition paths. In PES, two local minima may be connected via a single transition state if they are sufficiently close to each other in conformation space, and neighboring pairs of minima are separated by turning points through which minimum-barrier paths would pass in connecting these minima.[36] There also have been a number of many methods for finding transition paths.[37–44] The most instructive method is discrete path sampling which gives the fastest kinetic path between icosahedral and decahedral for LJ_{75} clusters.[37–40] The uphill and downhill walks method found pathways to transition states or dissociation channels from equilibrium structures on the potential energy surface.[44] Transition pathways in DNA were also described by using energy landscape.[41] Besides, a modification of the nudged elastic band method for finding minimum energy paths provides good preference by climbing up along the elastic band to converge rigorously on the highest turning point.[45]

Here we developed a Branched Dynamic Lattice Searching (B-DLS) method to travel the PES and describe it by a single-root network (SRN). By reserving the connections between structures of different conformations, the network connecting all the structures from a single root and the transition paths in PES is conveniently obtained. With this simplification, the local PES could be mapped into a SRN.

[a)]Author to whom correspondence should be addressed: clj@ustc.edu

II. METHOD

A. Potential energy function

As a benchmark system, the potential energy function of the cluster is based on the Lennard-Jones (LJ) model[46] which is very simple,

$$\mathrm{LJ}(r) = \varepsilon[(r_0/r)^{12} - 2(r_0/r)^6].$$

Here, r is the interatomic distance, r_0 is the equilibrium pair distance, and ε is the pair well depth. In this work, we set $\varepsilon = r_0 = 1$ to simplify the calculation, so the function can be simply written as

$$\mathrm{LJ}(r) = r^{-12} - 2r^{-6}.$$

B. Branched dynamic lattice searching (B-DLS)

To get sufficient visualization data, we need an efficient method to travel the PES. Among the most efficient algorithms,[47–60] the concept of Dynamic Lattice Searching (DLS) was used here.[54] However, to get details of the local PES, DLS was changed as B-DLS. Different from DLS, the optimization process of B-DLS will fork into many branches after each local optimization. As we can see in Fig. 1, the PES is composed of many local funnels, and each local funnel contains a number of basins. Here one local funnel represents one morphology and one basin represents one local minimum structure. Actually, traveling the PES is a process of relaxing the initial structure from the peak to the bottom of a funnel. It is obvious that the process needs two kinds of steps as labeled by red and blue arrows in Fig. 1. The red arrow means that the structure passes over the barrier to other local minimum (jump to other basin) and the blue arrow means that the structure executes local optimization to converge to local minimum (relax to the bottom of the basin). Here we give the details of these two steps to show how they work.

(1) For the initial structure, find all the vacancy sites in the surface of the initial structure and pick out the N_{mov} (the number of atoms that should be moved) atoms in the cluster with the highest energy. Then move these high-energy atoms to the N_{mov} vacancy sites generated from the surface lattice randomly. If energy of the new structure decreases, save it. This step should be tried many times to get better preference in relaxation. At the end of this step, the best N_{best} (the number of saved structures) new structures will be saved.

(2) However, the new structures are still less-optimized like the position of peak or the hillside that is far away from the bottom of the basin. Thus, in this phase, the new structures should be optimized by L-BFGS[61,62] to reach to the bottom in PES. After this step, the optimized structures will be sent to step 1 to repeat these two steps until there are no structures with lower energy.

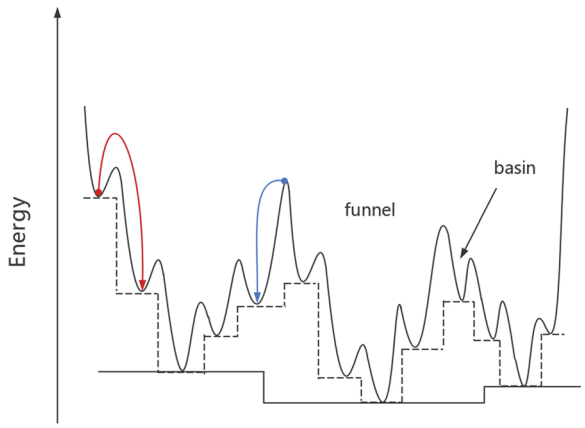

FIG. 1. Illustrations of two steps in traveling PES. The red arrow means jumping from one basin to another and the blue arrow means relaxation from the peak to the bottom.

By combining these two steps, the traveling of PES can be imagined as current flowing from the peak to the bottom of funnels. Here is a tip that this current will fork into many branches rather than flowing through only one path. One advantage of this forking is that the program can travel the PES as full as possible to get as many typical structures as possible. Besides, the forking makes finding the transition path between two structures possible.

1. Travelling the PES from single root

B-DLS starts from a random root structure, and the performance of SRN is based on the root. If the initial root structure lies in certain positions on PES, all possible low-energy morphologies (such as face centered cubic, icosahedral, and decahedral) can be located in a single B-DLS search. Thus, B-DLS search will be repeated many times from different random structures to choose a good root structure.

Then, re-travel the PES from the selected root structure and record all possible information during the B-DLS search. For convenience, here we use a queue to record the traveling. The flow chart of this step is given in Fig. 2.

(1) Put the initial structure into the queue to start the calculation.
(2) Next, taking the structure ejected from the queue as the father structure, perform dynamic lattice searching on this structure to generate N_{best} child structures.
(3) If the child structures are lower in energy than the father, add them to the queue. Besides, the relations between the child and father structures were saved at the same time.
(4) If the queue is empty, terminate this calculation and output the queue. Otherwise, jump to step (2).

2. Generate transition path on PES

Given two local minima, the program uses two steps to find the simple path between them. The first step is to find the turning point which has the highest energy in the transition path. The recursion algorithm was used to exhaust all ancestors of these two minima to find the turning point. The next step is finding the shortest path from the turning point to each local minimum. Here we give a simple example shown in Fig. 3 to explain how to generate the transition path between node1 and node6:

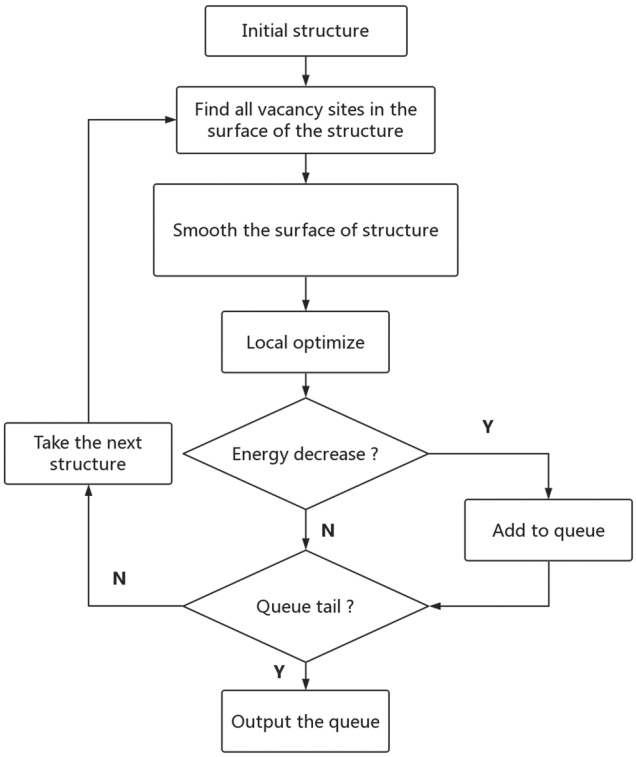

FIG. 2. Flow chart for algorithm of traveling PES.

(1) First, find the father nodes of node1 and node6 recursively. To node1, the set of ancestor nodes contains node2, node3, node4, and node5. To node6, the set of ancestor nodes contains node 7, node8, node4, node9, and node5.
(2) Next, take the intersection of these two sets which are signed as green nodes in Fig. 3. By selecting the lowest energy node (node4), the turning point in the transition path was determined.
(3) Repeatedly find fathers by the recursive algorithm to two start nodes until meet the turning point (node4). There is a tip that there may be more than one path reaching the turning point, and the program will save all these paths to minimize the length of the path.

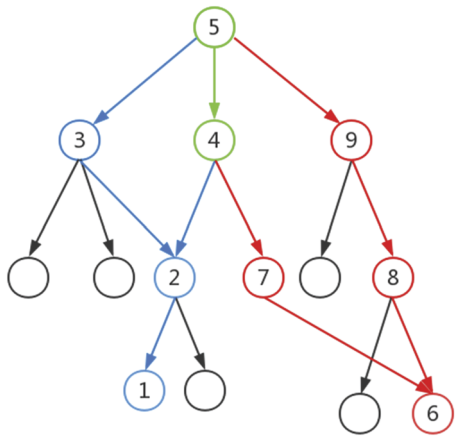

FIG. 3. A simple example to show how to generate the transition path. The starting nodes are node1 and node6. Nodes with same color and green nodes compose the set of ancestors.

(4) After completing the steps above, the transition path between node1 and node6 can be generated by selecting the shortest path. As one can see, the shortest path contains node1, node2, node4, node7, and node6.

C. Visualization

Visualizing SRN needs all path information obtained from the calculation. Herein, each path information entry means that the structure corresponding to the energy of the son could be derived from the father structure. First, exhaust all path entries and establish the node for each energy. Second, exhaust path entries again, at the same time, save the topological relation between them, and add the pointer of each son node to the father node. After this, the network has been established successfully. Next, count the number of the nodes without the son structure and allocate x axis to them by the sequence of establishing the node (the y-axis of the nodes is their energies). Then add the line connecting two nodes and set the size of a node proportional to the number of lines connecting to this node. Finally, label the transition paths by different colors and list the detailed transition path graphs. All visualization jobs were done by the matplotlib library of python.

III. RESULTS AND DISCUSSION

In SRN, each node at the end of the vertical line represents one structure and the nodes connected by lines mean that these two nodes can be transformed to each other by one DLS optimization. Besides, a diagonal which represents the node has been generated before, and the node at the top of this diagonal generates this node again. Herein, for convenience of expression, we call this phenomenon as a "jump," which actually means nothing in real. To check the performance of our method described above, we apply it to describe the PES of LJ_{38}, LJ_{55}, and LJ_{75} clusters, which were popular benchmarks in many methods.

A. LJ_{38}

The SRN of the LJ_{38}-cluster is plotted in Fig. 4(a), which is very complex due to the "jump" phenomenon. Thus, we merge the jump lines into the size of the nodes to increase the readability of this graph [plotted in Fig. 4(b)]. In Fig. 4(b), it is very easy to identify the local funnels under a vertical line. For example, the root structure generates three branches which can be regarded as three separated local funnels. Specially, the truncated octahedral locates in the third child branch of the second separated local funnel and the icosahedral locates in the third separated local funnel which is very narrow and deep. It is clearly noted that the local branches segregate these local minima, but at the same time we should realize that for the high-energy structures the jump lines connect them between branches very frequently. Thus, these structures can be considered as the overlap of these local branches.

Furthermore, the transition paths between typical morphologies in SRN can be sampled in detail. Figure 5 plots the detailed transition paths from icosahedral to truncated octahedral, icosahedral to icosahedral, and truncated octahedral to

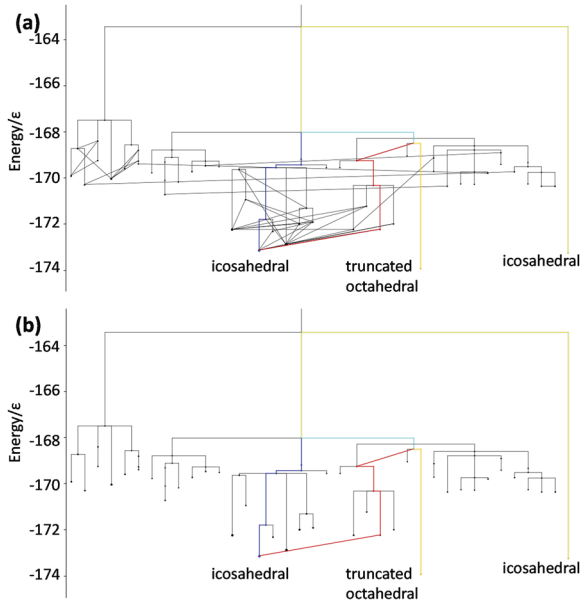

FIG. 4. The SRN of LJ_{38} (a) and the simplified SRN (b). Each node in SRN means a structure and the sizes of nodes in (b) represent the number of structures that generate the structure corresponding to the node. Each line in the SRN means that the upper structure can generate the nether structure by one optimization. The blue, red, and cyan lines give the paths between truncated octahedral and two icosahedral motifs.

icosahedral (as highlighted in Fig. 4 as red, blue, and cyan, respectively). In the transition path, the numbers in the square brackets near the red narrows mean the number of changed atoms between the father and son structure. The changed atoms are plotted in red and blue in son and father structures, respectively. The conformation between father and son structures represents the structure located to be lattice searching before local optimization. Besides, there are paths characterized by different colors in the SRN, and one tip is that the yellow path represents the repetitive parts of different paths.

If a morphology lies in a wider funnel, it will be visited more frequently, which is given in a larger node in SRN. Figure 6 plots the size of nodes as a function of energy. In agreement to literatures, the truncated octahedral funnel containing the global minimum (GM) is deep and narrow, and the icosahedral funnel is much wider.

B. LJ_{55}

When the number of local funnels and topological connections increase quickly, the SRN of LJ_{55}-cluster becomes more complex (Fig. 7). As shown in Fig. 7(a), the overlap between branches becomes gathered in some nodes such as Node1 and Node2. These two nodes and their descendants almost attract all jump lines from other branches. The phenomenon of merging child branches becomes increasingly obvious. Besides, the funnel of GM is no longer relatively narrow and steep because the size of the node corresponding to the GM is larger than many other nodes which mean that this conformation is easy to be found.

The transition path between icosahedral and fcc is plotted in Fig. 8 and it takes six steps. It is well known that LJ_{55} can be seen as a single funnel landscape. In our method, it is also very easy to locate the GM structure of LJ_{55} due to its single funnel feature. As shown in Fig. 9, the icosahedral GM structure is visited very frequently. However, there still are some other morphologies in LJ_{55}, such as decahedral, fcc, and tetrahedral. Each morphology represents one local funnel, although these local funnels are relatively narrow and shallow in LJ_{55}.

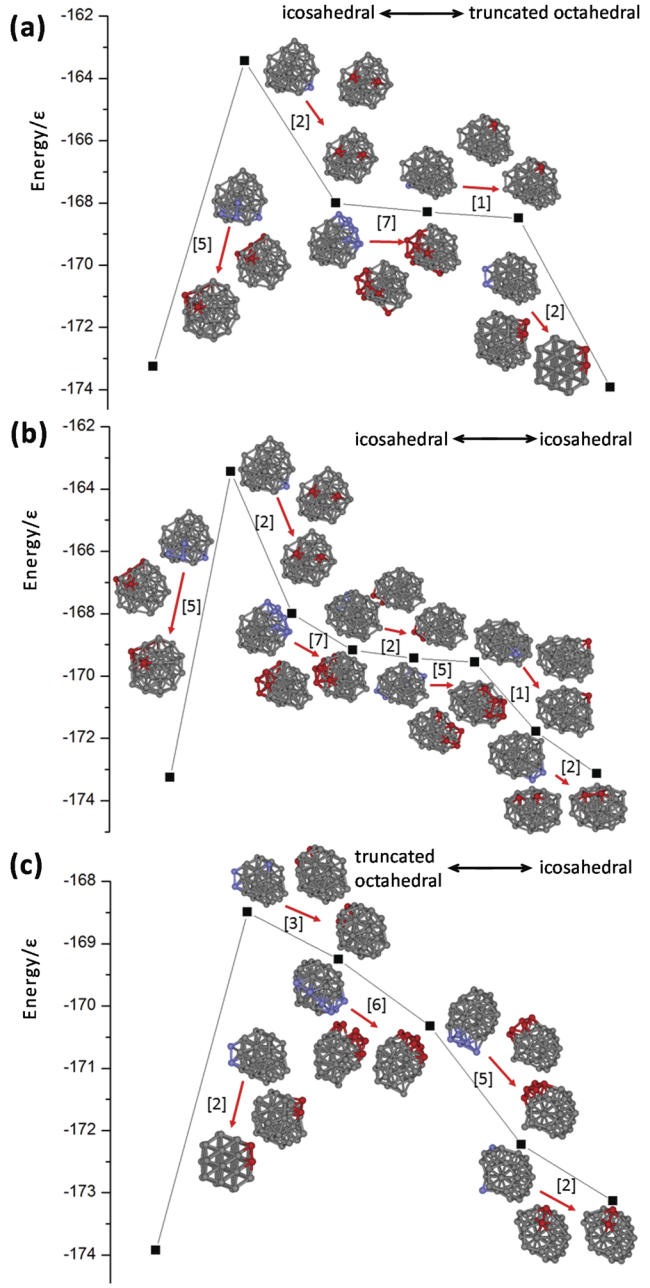

FIG. 5. Transition paths between LJ_{38} clusters: (a) icosahedral to truncated octahedral; (b) icosahedral to icosahedral; and (c) truncated octahedral to icosahedral. The numbers in the square brackets mean the number of changed atoms between the father and son structure. The changed atoms were plotted as red in the son structure and as blue in the father structure. The conformation between the father and son structure represents the structure which has a smoothed surface but is not locally optimized by the algorithm.

C. LJ_{75}

When analyzing the SRN of the LJ_{75} cluster plotted in Fig. 10, the network becomes more characteristic.

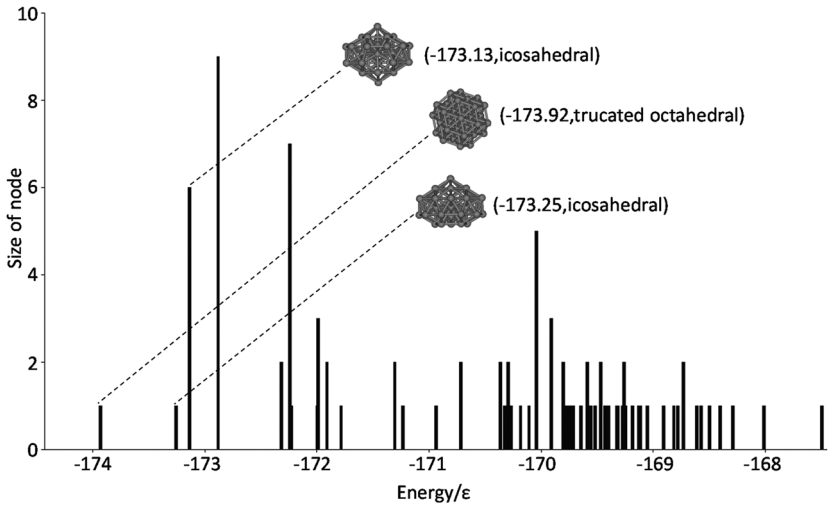

FIG. 6. Bar chart illustrating the size of each node in LJ_{38}. The horizontal coordinate represents the energy of each structure. The vertical coordinate means how many structures generate the structure corresponding to the horizontal coordinate (also means the size of the node in the simplified SRN). For example, there are six structures which generate the icosahedral (−173.13).

The proportion of jump lines between separated local funnels decreases significantly, which indicates that jump lines mainly distribute on the inside of two funnels. Due to the high complexity, it is very difficult to describe the shape of the funnel in detail in full SRN [Fig. 10(a)]. From the simplified SRN [Fig. 10(b)], each branch has many child branches which correspond to large nodes in the graph and there is a lot of overlap between the child branches. However, although this

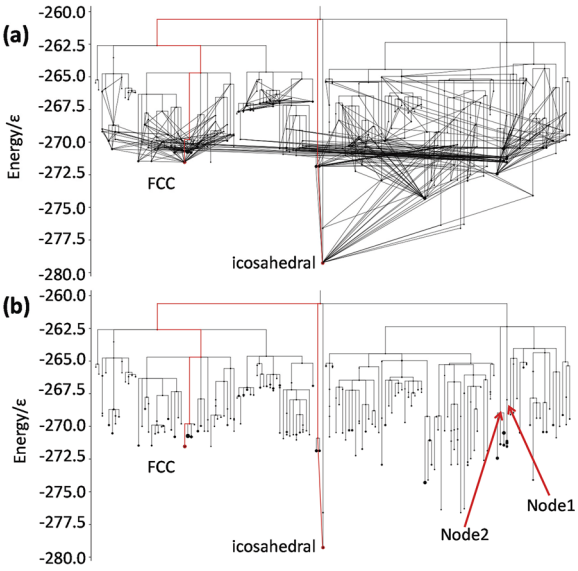

FIG. 7. The SRN of LJ_{55} (a) and the simplified SRN (b). The path between icosahedral and FCC is given in red.

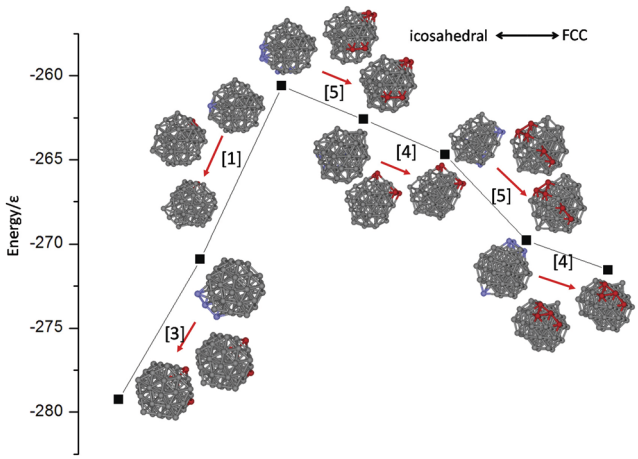

FIG. 8. The transition path between icosahedral and FCC in LJ_{55}.

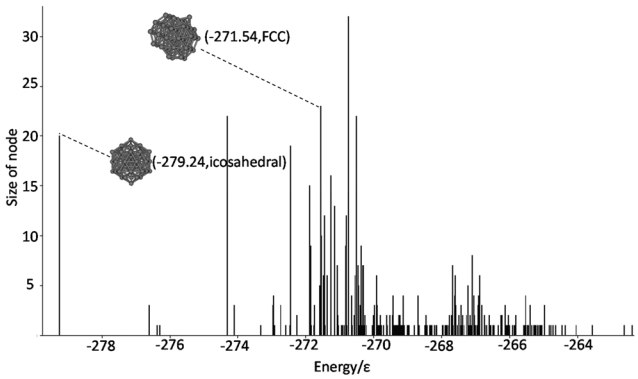

FIG. 9. Bar chart illustrating the size of each node in LJ_{55}.

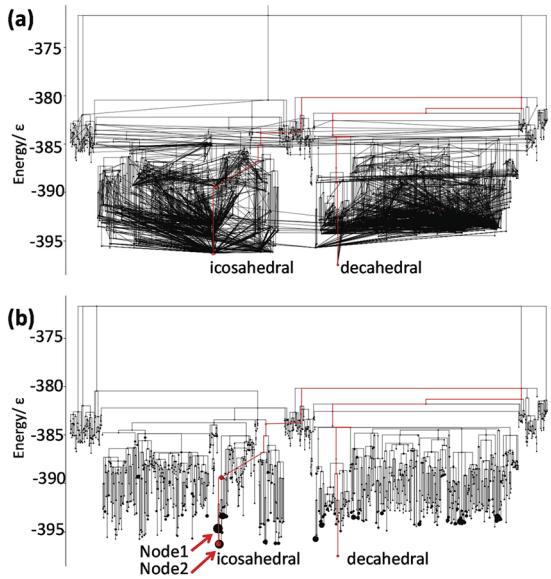

FIG. 10. The SRN of LJ_{75} (a) and the simplified SRN (b). The path between decahedral and icosahedral is given in red.

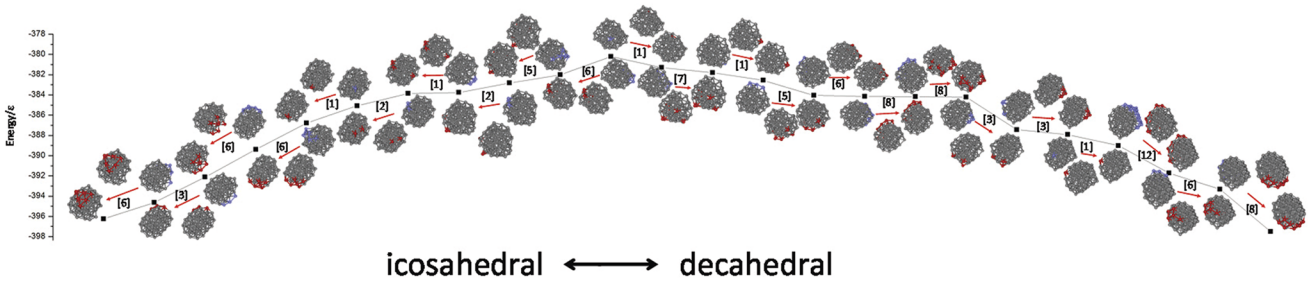

FIG. 11. The transition path between icosahedral and decahedral in LJ_{75}.

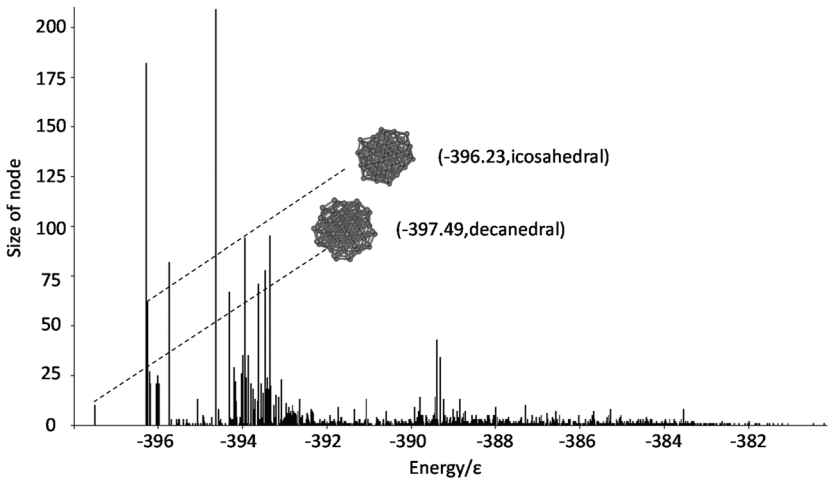

FIG. 12. Bar chart illustrating the size of each node in LJ_{75}.

network has been simplified, SRN still cannot give the exact shape of local funnels due to the complexity. There are some "hot" structures which have very large nodes in SRN [such as Node1 and Node2 labeled in Fig. 10(b)], indicating wide funnels. However, the GM locates in a small funnel which seems very hardly to reach.

The transition path between icosahedral and decahedral is plotted in Fig. 11, which takes twenty three steps indicating high difficulty in structural transition. As shown in Fig. 11, the decahedral GM structure is visited much less frequently than the icosahedral structures despite its low energy, which is in good agreement with previous studies.

D. Discussions

From the SRN, it is easy to find some patterns to understand the PES. The PES of LJ clusters at different sizes display characteristic features. For example, LJ_{38} and LJ_{75} clusters show double-funnel feature in PES, and the GM funnel is narrow and deep. However, the LJ_{55} cluster shows single-funnel feature, and the GM funnel is wide and deep. These results are consistent with other benchmark calculations in literatures. With the growth of cluster sizes, SRN becomes complex because the number of local minima and topological connections between local funnels increase quickly. The jumps between funnels lie only in high-energy areas because only structures with hybrid morphology can be branched into different funnels. With the growth of cluster sizes, the complexity and the independence of each local funnel increase dramatically. The decrease of jump lines between local funnels means that the funnels may be far away from each other so that the connection between them is hard (Fig. 12).

It should be noted that the paths in SRNs are based on dynamic lattice searching, where the connection of two structures can be taken as a "tunnel" without any thermodynamic or kinetic meaning. Thus, transition in SRN is somewhat a physical hard path in PES, which is different from the Monte Carlo based methods, such as the discrete path sampling method.[37–40] Due to the high complexity, PES cannot be described directly, and each method has its own shortness. Although only physical hard path can be given in SRN, it gives an alternative way to understand the global feature of PES and has its own special viewpoint.

IV. CONCLUSIONS

In conclusion, we travel the PES by B-DLS and characterize the PES of LJ_{38}, LJ_{55}, and LJ_{75} clusters by SRN. In addition, the details of transition from one morphology to another were demonstrated successfully. By gathering the topological relations, SRN explains some phenomena in searching PES such as the difficulty of locating GM structures. Furthermore, the topological relations in SRN simplify the complexity of PES significantly by turning the number of lines into the size of each node. On the whole, the SRN abandon some insignificant information and give a simplified view of local PES. Benefitting from this, more details about typical morphologies can be shown clearly and this may be useful to get new findings about PES. The transition path demonstrates the details

of transition between two structures. Actually, each transition path is a convex curve which represents a structure jump from one energy trap to another and each step in path shows the movement of atoms clearly. These paths may contribute to understanding the mechanism of changes between different morphologies. Although SRN gives only physical hard paths in PES, it gives an alternative way to understand the global feature of the complex PES.

ACKNOWLEDGMENTS

This work is financed by the National Natural Science Foundation of China (Grant Nos. 21573001 and 21873001) and by the Foundation of Distinguished Young Scientists of Anhui Province.

[1]B. A. Waite and W. H. Miller, J. Chem. Phys. **74**, 3910 (1981).
[2]M. A. Collins, Theor. Chem. Acc. **108**, 313 (2002).
[3]P. Hay, R. Pack, R. Walker, and E. Heller, J. Phys. Chem. **86**, 862 (1982).
[4]M. Iannuzzi, A. Laio, and M. Parrinello, Phys. Rev. Lett. **90**, 238302 (2003).
[5]D. J. Wales, M. A. Miller, and T. R. Walsh, Nature **394**, 758 (1998).
[6]S. Goedecker, J. Chem. Phys. **120**, 9911 (2004).
[7]M. T. Oakley and R. L. Johnston, J. Chem. Theory Comput. **10**, 1810 (2014).
[8]M. T. Oakley and R. L. Johnston, J. Chem. Theory Comput. **9**, 650 (2012).
[9]M. T. Oakley, D. J. Wales, and R. L. Johnston, J. Phys. Chem. B **115**, 11525 (2011).
[10]M. A. Miller and D. J. Wales, J. Chem. Phys. **111**, 6610 (1999).
[11]A. R. Dinner, A. Šali, L. J. Smith, C. M. Dobson, and M. Karplus, Trends Biochem. Sci. **25**, 331 (2000).
[12]S. V. Krivov and M. Karplus, Proc. Natl. Acad. Sci. U. S. A. **101**, 14766 (2004).
[13]M. Lieberman, M. Tabet, and T. Sasaki, J. Am. Chem. Soc. **116**, 5035 (1994).
[14]S. V. Krivov and M. Karplus, J. Chem. Phys. **117**, 10894 (2002).
[15]Y. Fukunishi, Y. Mikami, and H. Nakamura, J. Phys. Chem. B **107**, 13201 (2003).
[16]S. C. Tucker and D. G. Truhlar, J. Am. Chem. Soc. **112**, 3338 (1990).
[17]B. C. Garrett, D. G. Truhlar, A. F. Wagner, and T. H. Dunning, Jr., J. Chem. Phys. **78**, 4400 (1983).
[18]B. C. Garrett and D. G. Truhlar, J. Chem. Phys. **72**, 3460 (1980).
[19]T. Joseph, R. Steckler, and D. G. Truhlar, J. Chem. Phys. **87**, 7036 (1987).
[20]C. Longjiu, C. Wensheng, and S. Xueguang, ChemPhysChem **8**, 569 (2007).
[21]J. P. K. Doye, Phys. Rev. Lett. **88**, 238701 (2002).
[22]I. Bytheway and D. L. Kepert, J. Math. Chem. **9**, 161 (1992).
[23]F. H. Stillinger and D. K. Stillinger, J. Chem. Phys. **93**, 6013 (1990).
[24]P. A. Braier, R. S. Berry, and D. J. Wales, J. Chem. Phys. **93**, 8745 (1990).
[25]Y. Feng, L. Cheng, and H. Liu, J. Phys. Chem. A **113**, 13651 (2009).
[26]F. H. Stillinger and D. K. Stillinger, J. Chem. Phys. **93**, 6106 (1990).
[27]S. V. Krivov and M. Karplus, J. Phys. Chem. B **110**, 12689 (2006).
[28]H. Busnengo, A. Salin, and W. Dong, J. Chem. Phys. **112**, 7641 (2000).
[29]C. P. Massen and J. P. Doye, Phys. Rev. E **71**, 046101 (2005).
[30]O. M. Becker and M. Karplus, J. Chem. Phys. **106**, 1495 (1997).
[31]G. J. Rylance, R. L. Johnston, Y. Matsunaga, C.-B. Li, A. Baba, and T. Komatsuzaki, Proc. Natl. Acad. Sci. U. S. A. **103**, 18551 (2006).
[32]S. Sato, J. Chem. Phys. **23**, 592 (1955).
[33]T. Komatsuzaki, K. Hoshino, Y. Matsunaga, G. J. Rylance, R. L. Johnston, and D. J. Wales, J. Chem. Phys. **122**, 084714 (2005).
[34]J. P. K. Doye, M. A. Miller, and D. J. Wales, J. Chem. Phys. **111**, 8417 (1999).
[35]D. J. Wales, J. Chem. Phys. **142**, 130901 (2015).
[36]J. M. Carr, S. A. Trygubenko, and D. J. Wales, J. Chem. Phys. **122**, 234903 (2005).
[37]D. J. Wales, *Energy Landscapes* (Cambridge University Press, 2003).
[38]D. J. Wales, Int. Rev. Phys. Chem. **25**, 237 (2006).
[39]D. J. Wales, Mol. Phys. **100**, 3285 (2002).
[40]D. J. Wales, Mol. Phys. **102**, 891 (2004).
[41]D. Chakraborty and D. J. Wales, J. Phys. Chem. Lett. **9**, 229 (2017).
[42]X.-J. Zhang, C. Shang, and Z.-P. Liu, J. Chem. Theory Comput. **9**, 5745 (2013).
[43]C. Shang and Z.-P. Liu, J. Chem. Theory Comput. **9**, 1838 (2013).
[44]K. Ohno and S. Maeda, Chem. Phys. Lett. **384**, 277 (2004).
[45]G. Henkelman, B. P. Uberuaga, and H. Jónsson, J. Chem. Phys. **113**, 9901 (2000).
[46]J. Lennard-Jones, Proc. R. Soc. London A **109**, 584 (1925).
[47]J. Wang, G. Wang, and J. Zhao, Phys. Rev. B **66**, 035418 (2002).
[48]J. Zhao, A. Buldum, J. Han, and J. Ping Lu, Phys. Rev. Lett. **85**, 1706 (2000).
[49]D. J. Wales and H. A. Scheraga, Science **285**, 1368 (1999).
[50]D. J. Wales and J. P. Doye, J. Phys. Chem. A **101**, 5111 (1997).
[51]J. Doye and D. Wales, Z. Phys. D: At., Mol. Clusters **40**, 194 (1997).
[52]L. Cheng, W. Cai, and X. Shao, Chem. Phys. Lett. **389**, 309 (2004).
[53]R. L. Johnston, Dalton Trans. **0**, 4193 (2003).
[54]L. Cheng, Y. Feng, J. Yang, and J. Yang, J. Chem. Phys. **130**, 214112 (2009).
[55]Z.-P. Liu and P. Hu, Top. Catal. **28**, 71 (2004).
[56]H. Fu, Z.-P. Liu, Z.-H. Li, W.-N. Wang, and K.-N. Fan, J. Am. Chem. Soc. **128**, 11114 (2006).
[57]G. Rossi, R. Ferrando, A. Rapallo, A. Fortunelli, B. C. Curley, L. D. Lloyd, and R. L. Johnston, J. Chem. Phys. **122**, 194309 (2005).
[58]A. Rapallo, G. Rossi, R. Ferrando, A. Fortunelli, B. C. Curley, L. D. Lloyd, G. M. Tarbuck, and R. L. Johnston, J. Chem. Phys. **122**, 194308 (2005).
[59]S. Darby, T. V. Mortimer-Jones, R. L. Johnston, and C. Roberts, J. Chem. Phys. **116**, 1536 (2002).
[60]C. Roberts, R. L. Johnston, and N. T. Wilson, Theor. Chem. Acc. **104**, 123 (2000).
[61]D. C. Liu and J. Nocedal, Math. Program. **45**, 503 (1989).
[62]R. H. Byrd, P. Lu, J. Nocedal, and C. Zhu, SIAM J. Sci. Comput. **16**, 1190 (1995).